Electrochemistry Communications 130 (2021) 107110

Contents lists available at ScienceDirect

Electrochemistry Communications

journal homepage: www.elsevier.com/locate/elecom

Effective electroosmotic transport of water in an intrinsically microporous polyamine (PIM-EA-TB)

Zhongkai Li [a], Richard Malpass-Evans [b], Neil B. McKeown [b], Mariolino Carta [c], Klaus Mathwig [d], John P. Lowe [e], Frank Marken [a,*]

[a] Department of Chemistry, University of Bath, Claverton Down, Bath BA2 7AY, UK
[b] EaStCHEM, School of Chemistry, University of Edinburgh, Joseph Black Building, David Brewster Road, Edinburgh, Scotland EH9 3JF, UK
[c] Department of Chemistry, Swansea University, College of Science, Grove Building, Singleton Park, Swansea SA2 8PP, UK
[d] Stichting imec Nederland within OnePlanet Research Center, Bronland 10, 6708 WH Wageningen, The Netherlands
[e] University of Bath, Materials & Chemical Characterisation Facility MC^2, Bath BA2 7AY, UK

ARTICLE INFO

Keywords:
Microporosity
Voltammetry
Electroosmosis
Desalination
Solar water harvesting

ABSTRACT

Tertiary-amine-based Polymers of Intrinsic Microporosity (PIMs) provide a class of highly porous molecularly rigid materials for the electrochemical transport of both ionic and neutral species. Here, the transport of water molecules together with chloride anions (i.e. the electroosmotic drag coefficient) is studied for the intrinsically microporous polyamine PIM-EA-TB immersed in aqueous 0.01 M NaCl (i) when protonated for pH < 4 or (ii) when not protonated for pH > 4. Preliminary data suggest that in both cases a high electroosmotic drag coefficient is observed based on direct H_2O transport into a D_2O-filled compartment (quantified by ^{1}H-NMR). For PIM-EA-TB there is a strong pH dependence with a higher electroosmotic drag coefficient in less acidic solutions (going from approx. 400 H_2O per anion at pH 3 to approx. 4000 H_2O per anion at pH 7), although the underlying absolute rate of water transport at a fixed voltage of −1 V appears to be essentially pH independent. Water transport through the PIM-EA-TB microchannels is rationalised based on the relative populations of chloride anions and of water in the micropores (essentially a 'piston' mechanism).

1. Introduction

Water transport and water purification with membranes represent important aspects of technologies that are key to societal challenges such as clean water provision and water harvesting [1], industrial water usage and recycling [2], and reliable irrigation in agriculture [3]. In order to purify water a plethora of technologies have been developed based on either (i) removing impurities and salts from water (e.g. using capacitive deionisation [4] or electrodialysis linked to renewable energy [5]) or (ii) extracting water from an impure resource (e.g. reverse osmosis [6] or forward osmosis [7]). Electrodialysis is a technique based on ion transport through a membrane and an important side effect of electrodialysis is electroosmosis, the transport of neutral species that accompany ionic species, for example in electroosmotic pumps [8]. Some materials have been designed to minimise electroosmotic transport (e.g. in commercial membranes [9,10]) but in other cases electroosmotic transport has been maximised (e.g. in modified silicates [11]). Here, electroosmotic transport of water is investigated in a polymer of intrinsic microporosity (PIM [12]).

PIMs have emerged as a special class of highly processable, highly porous, and glassy polymers with a high free volume based on a molecularly rigid backbone structure [13]. The ability of PIMs to dissolve in common organic solvents makes them ideal for the deposition and study of thin films [14] and for the study of membrane transport phenomena. Here, PIM-EA-TB (Fig. 1A) is investigated. When depositing PIM-EA-TB onto a laser-machined microhole in an inert polymer substrate (or an array of 10 × 10 microholes, see Fig. 1C) and placing the resulting membrane between two electrolyte-solution-filled compartments (Fig. 1B), ion transport and ion current rectification phenomena have been observed [15]. Ionic currents are rectified due to the microhole restricting access to one side of the ionomer coating. In combination with semi-permeable ion transport in PIM-EA-TB, this results in asymmetric concentration polarisation [16] and a switch between an "open" diode state (electrolyte accumulates in the microhole to give a low resistance) and a "closed" diode state (electrolyte in the microhole is depleted to give a high resistance). It is shown here that this

* Corresponding author.
E-mail address: f.marken@bath.ac.uk (F. Marken).

https://doi.org/10.1016/j.elecom.2021.107110

Available online 18 August 2021

ionic current rectification is associated with rectified electroosmotic pumping.

Rectified electroosmotic transport in nanopore ionic diodes has been reported by White and coworkers [17] and demonstrated by Martin and coworkers [18,19]. Here, a microscale ionic diode based on PIM-EA-TB is employed and the electroosmotic flow for the open/closed diode state is quantified. The rigid microporous structure of PIM-EA-TB is suggested to be responsible for the very high rate of water transport with electroosmotic drag coefficients of up to 4000 (compared to 13,000 in porous silica reported by Shin et al. [20] or approximately 1 for Nafion-based membranes [21]).

2. Experimental

2.1. Chemical reagents

The PIM-EA-TB polymer was prepared with 70 KD molecular weight following a previously reported method [22]. Agarose powder was purchased from Melford Ltd. Dimethyl sulfoxide (HPLC, 99.7%) was purchased from Honeywell. Chloroform and D_2O (99.9 atom% D) were purchased from Sigma-Aldrich. Sodium chloride (99.5%) and hydrochloric acid were purchased from Fisher Scientific Ltd. All chemicals were utilised without further purification. Aqueous solutions were prepared with ultra-pure water from a Thermo Scientific water purification system, with a resistivity not$<$18.2 MΩ cm (20 ℃).

2.2. Instrumentation

Electrochemical experiments were performed on a program-controlled potentiostat (Autolab PGSTAT12) in a four-electrode configuration (working, sense, counter, and reference electrodes [17]). A membrane electrochemical cell (U-cell, Fig. 1B) was constructed in which a membrane-coated, laser-drilled Teflon substrate (5 μm thick) separated two cylindrical half cells (diameter 0.5 in.). Carbon rods were used as working and counter electrodes, and silver wires served as quasi-sense and quasi-reference electrodes. During the electrochemical tests, the working and sense electrodes were always placed on the membrane side of the cell. The detection of H_2O in D_2O was performed by ^{1}H-NMR spectrometry (Bruker 400 MHz) employing DMSO as an internal standard.

2.3. Procedures

Immobilisation of a PIM-EA-TB film on a Teflon substrate. A Teflon substrate with a laser-drilled micropore array was prepared with a thickness of 5 μm (Laser Machining Ltd, Birmingham, UK). Fig. 1C shows the optical microscopy images of an array of microholes with 10 μm diameter and 200 μm pitch. To prepare the membrane, 30 μL 3 mg/mL solution of PIM-EA-TB in chloroform was deposited asymmetrically onto the laser-drilled Teflon substrate on a glass substrate (the glass substrate was initially coated with a thin layer of 1% wt. agarose gel [23] to prevent the PIM-EA-TB solution from penetrating through the microholes). After evaporating, a uniform membrane coating was formed over the array region with a thickness estimated to be typically 10 ± 5 μm [24]. The membrane was then pre-treated in aqueous HCl at pH 2 for 1 h, rinsed, and finally immersed in 0.01 M NaCl solution with the required pH for 2 h before performing experiments.

Electrochemical experiments and Nuclear Magnetic Resonance (^{1}H -MR) monitoring. Although the *in situ* ^{1}H -NMR measurement of electrophoretic water transport has been reported [25], here a simple approach based on taking samples from the electrochemical cell and transfer of H_2O into D_2O is employed. A volume of 8 mL 0.01 M NaCl in H_2O solution was added to the working electrode compartment (pH adjusted with 10 mM HCl as required; a constant ionic strength was maintained up to the data point for 10 mM HCl at pH 2.2; data points for pH 2 were obtained by addition of 1 M HCl to give approximately twice the ionic strength). A volume of 8 mL 0.01 M NaCl in D_2O solution was added to the counter electrode compartment, with 3.1 mM DMSO added as an internal ^{1}H -NMR standard (2.0 μL DMSO in 10 mL D_2O). During measurements, the cell was first allowed to stand for 40 min without any applied voltage. The diffusional transport of H_2O into the D_2O compartment was monitored. Then a fixed voltage of −1 V (consistent with an open diode) was applied to the membrane for 80 min while measuring H_2O transport at 20-minute intervals. Finally, the cell was again allowed to rest without applied voltage for 40 min while monitoring H_2O transport. Every 20 min, a sample of 0.6 mL D_2O solution was taken from the counter electrode compartment (ensuring good mixing before samples were taken). The samples were then measured by ^{1}H -NMR (by integration of peaks at 2.65 ppm for DMSO and at 4.70 ppm for protons in H_2O/D_2O) to analyse the change of H_2O concentration in D_2O. From the ^{1}H -NMR and electrochemical data the coefficient of electroosmotic drag (the number of water molecules being transported per anion) was determined.

3. Results and discussion

3.1. Electroosmotic transport in anionic diodes based on microporous polyamine: Voltammetry

The cyclic voltammetric characteristics for PIM-EA-TB coated over a single 10 μm diameter microhole and immersed in 10 mM NaCl has been reported previously [23]. Fig. 2A shows a typical set of data with low

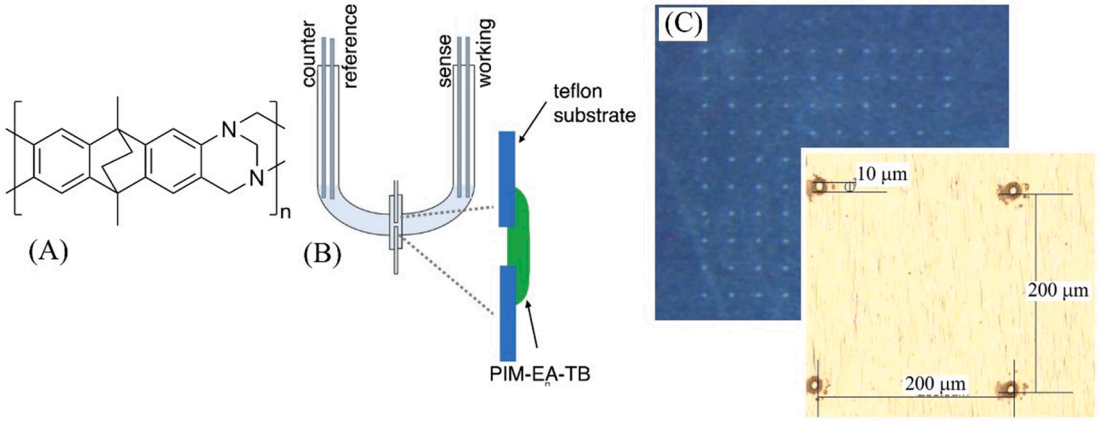

Fig. 1. (A) Molecular structure of PIM-EA-TB. (B) Four-electrode membrane voltammetry experimental configuration. (C) Optical micrographs showing the 10 × 10 microhole array and individual microholes with 10 μm diameter and 200 μm pitch in a Teflon substrate 5 μm thick.

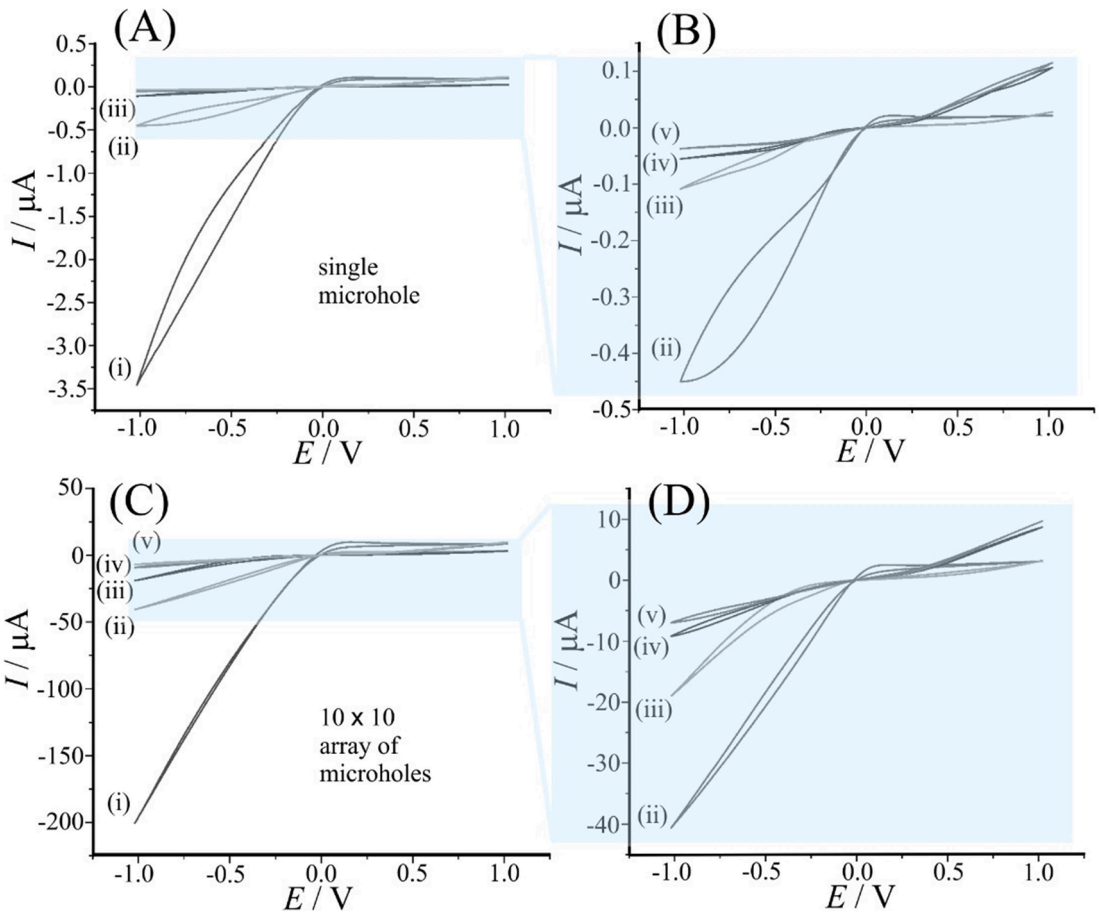

Fig. 2. (A,B) Cyclic voltammetry data (scan rate 0.2 Vs^{-1}) for a 10 μm microhole covered with PIM-EA-TB and immersed in aqueous 10 mM NaCl at various pH values: (i) 2, (ii) 3, (iii) 4, (iv) 5, and (v) 6. (C,D) as before but for a 10 × 10 array of microholes.

currents in the positive potential range (the diode is closed) and higher currents in the negative potential range (the diode is open). This behaviour is consistent with that previously reported for an anionic diode [26] and has been further investigated by Chen and coworkers [27,28]. A pre-condition for the current rectification effect is semi-permeability, which is achieved when the PIM-EA-TB is protonated. Cyclic voltammetry data for pH values of 2, 3, 4, 5, and 6 are shown in Fig. 2A and 2B, and the rectification effect clearly weakens with increasing pH values. At pH 2, the anionic diode is open in the negative potential range and closed in the positive potential range.

Data for a similar experiment performed with a 10 × 10 array of 10 μm diameter microholes in a 5 μm thick Teflon substrate are shown in Fig. 2C and 2D. Currents for the array generally increase by approximately two orders of magnitude, consistent with the anticipated increase in active area. The trends associated with pH are very similar for the single microhole and for the array measurements. Some minor variation in current–potential characteristics are likely to be explained mainly by variations in the PIM-EA-TB film deposition and film thickness. Due to the relatively high scan rate of 0.2 V s^{-1} some degree of non-steady-state behaviour is observed and further investigated in chronoamperometry experiments.

Fig. 3 shows chronoamperometry data for a single microhole (3A and 3B) and for an array of microholes (3C and 3D). The rectification effect is most clearly detected at pH 2 and the switching time for the anionic diode is typically 10 s and 30 s for a single microhole or array, respectively. When changing the pH to less acidic conditions, transient features become more complicated (a combination of rising and falling transient components can be observed due to different processes contributing) and the rectification effect is lost. Contributions to the current transients are likely from diffusion-migration, from compositional changes within the PIM-EA-TB, and from electroosmotic phenomena that occur simultaneously (*vide infra*). Next, the significance of electroosmotic flow and the effect of pH on the electroosmotic transport of water in PIM-EA-TB are investigated.

3.2. *Electroosmotic transport in anionic diodes based on microporous polyamine: Water transport*

Experiments exploring the transport of water were based on ^{1}H NMR determination of the H_2O content when placing D_2O solution into the counter electrode compartment (see Fig. 4A). A Teflon membrane with a 10 × 10 array of 10 μm diameter microholes was employed, covered with PIM-EA-TB approximately 10 μm thick on the side of the working electrode. In this configuration, the "open state" of the ionic diode with anion transport is observed at negative applied potentials (Fig. 4A). A typical data set for changes in water concentration in the counter electrode compartment as a function of time is shown in Fig. 4B (for pH = 3). Phases 1 and 3 correspond to periods of time with no applied bias and therefore reflect freely diffusing water. Phase 2 reflects the transport with −1 V applied voltage, showing clearly enhanced transport of water from the H_2O compartment into the D_2O compartment. Note that these are preliminary data and that in future more data points collected over a longer period of time will help to improve data quality. When repeating this experiment with + 1 V applied bias, only insignificant water transport occurs (within the diffusional background), consistent with rectified water transport in the diode.

The analysis of the diffusion of water from the H_2O compartment into the D_2O compartment was performed without applied potential and

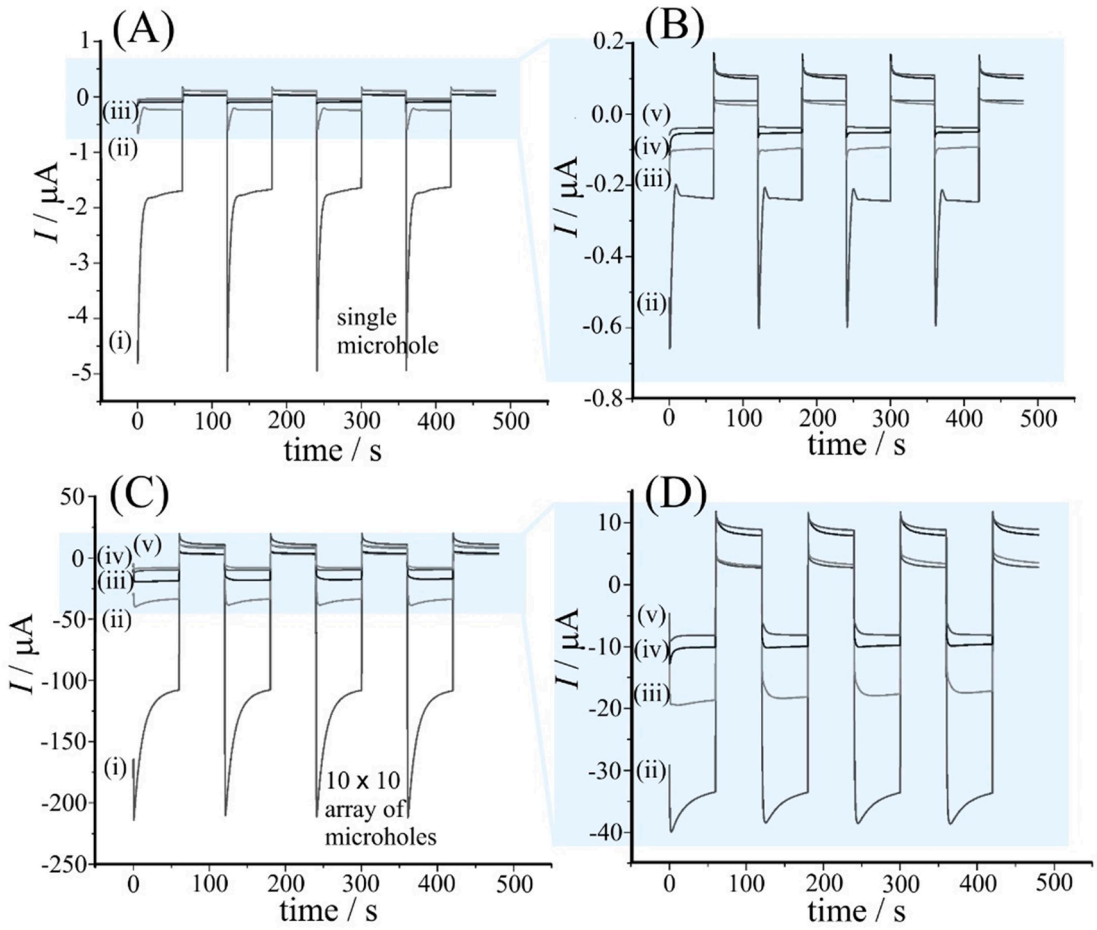

Fig. 3. (A,B) Chronoamperometry data (stepping the potential between −1 V and + 1 V) for a 10 µm microhole covered with PIM-EA-TB and immersed in aqueous 10 mM NaCl at various pH values: (i) 2, (ii) 3, (iii) 4, (iv) 5, and (v) 6. (C,D) as before but for a 10 × 10 array of microholes.

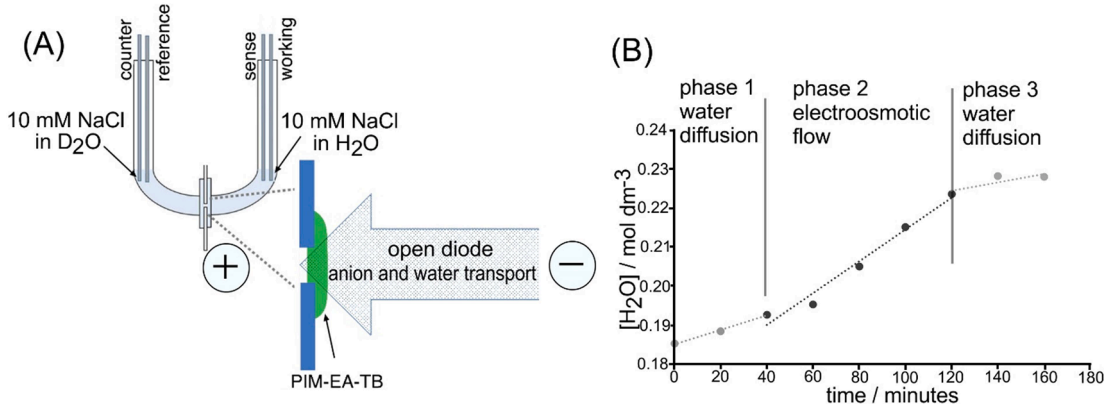

Fig. 4. (A) Illustration of the experimental cell with 10 mM NaCl in H_2O in the working electrode compartment and 10 mM NaCl in D_2O in the counter electrode compartment. With negative applied bias anion transport occurs with H_2O transport into the D_2O. (B) Plot of the [H_2O] concentration in the counter electrode compartment as a function of time with phases 1 and 3 without applied bias and phase 2 with −1 V bias.

with 10 independent data sets (see Fig. 5A) suggesting an average diffusional flux density of 3.8 ± 1.5 mol m^{-2} s^{-1} for water (H_2O into D_2O), essentially independent of the solution pH. The considerable error margin is likely to be linked to a variation in the thickness of the PIM-EA-TB film but also to additional effects from unintended variations in hydrostatic pressure. The diffusional flux density gives an average of $D_{H_2O,PIM} = 0.6 \pm 0.3 \times 10^{-9}$ m^2 s^{-1} (assuming a water flux density = Dc/δ with an average PIM-EA-TB thickness of typically $\delta = 10$ µm, employing $c = 56 \times 10^3$ mol m^{-3} as the H_2O concentration difference, and using $D_{H_2O,PIM}$ as the diffusion coefficient of water in the PIM-EA-TB). This value compares to the self-diffusion coefficient for water of approximately $D_{H_2O,WATER} = 2.3 \times 10^{-9}$ m^2 s^{-1} at room temperature [29,30] and is evidence for somewhat slower but still significant self-diffusion of water molecules within the PIM environment. Note that differences between D_2O and H_2O, for example in cohesion energy and importantly in the rate of self-diffusion [31], suggest that this comparison is valid only in approximation. The average transit time under these conditions for water molecules based purely on diffusion can be estimated as $\delta^2/2D$

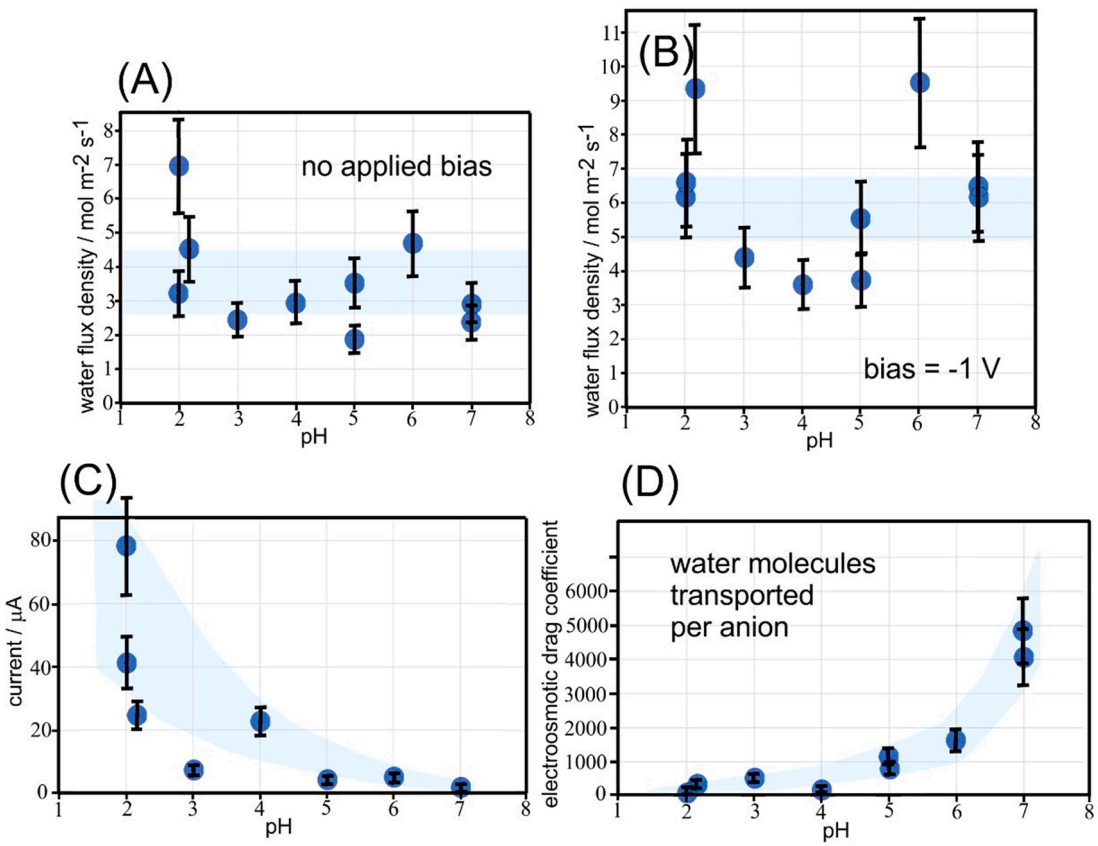

Fig. 5. (A) Plot of water flux density in mol m^{-2} s^{-1} versus pH without applied potential. (B) Plot of water flux density versus pH at −1 V bias with the diffusional water flux density subtracted. (C) Plot of the average ion current (averaged over 80 min) versus pH. (D) Plot of electroosmotic drag coefficient (the number of water molecules transported through the PIM-EA-TB per chloride anion) versus pH. Estimated error bars ± 20% are indicated. Blue lines are provided to guide the eyes. (For interpretation of the references to colour in this figure legend, the reader is referred to the web version of this article.)

$= \tau = 0.1$ s.

With an applied bias of −1 V, the transport rate of water increases due to the electroosmotic flux. Fig. 5B summarises the trend in electroosmotic water flux density for water transport (with the underlying diffusional water flux density subtracted). Electroosmotic water transport amounts to a flux density of approximately 5.8 ± 1.8 mol m^{-2}

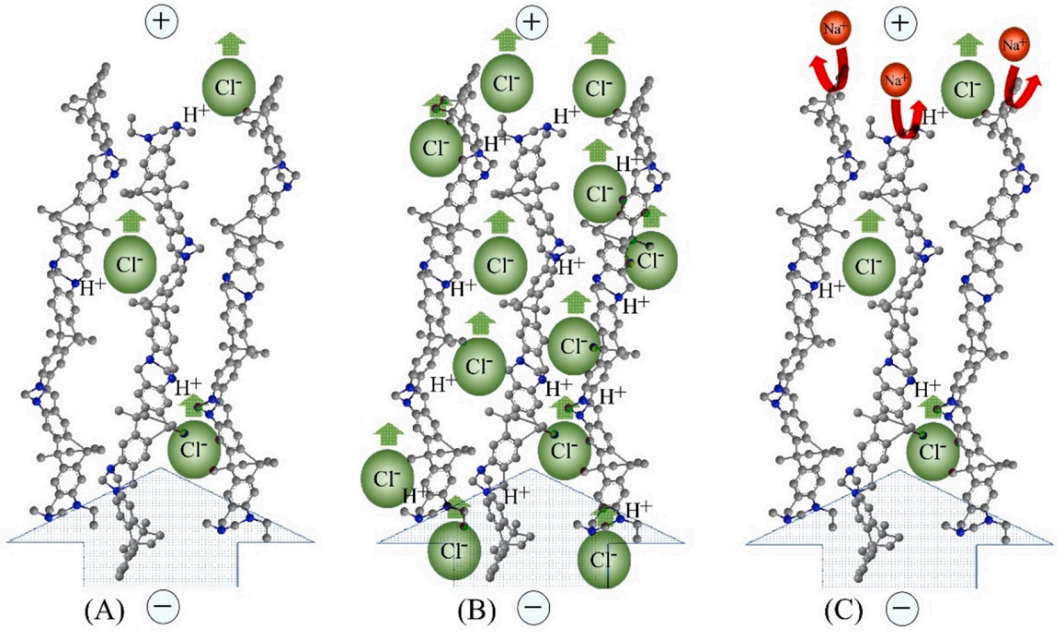

Fig. 6. Schematic diagram (not to scale) illustrating anion and water transport for (A) pH > 4 with partial protonation, (B) pH < 4 with a higher degree of protonation, and (C) the situation where cations try to enter the microporous PIM-EA-TB against the water flow.

s^{-1} (Fig. 5B). Thus, the electroosmotic water flow more than doubles the total observed water transport. Perhaps surprisingly, this water flux is not strongly affected by pH (Fig. 5B) in spite of the anticipated effects due to polymer protonation with approximately $pK_A \approx 4$ [23].

In acidic conditions, the ionic current is dominated by anions due to the protonation of the tertiary-amine sites in the PIM-EA-TB polymer backbone [23]. This allows the current to be interpreted as anion (chloride) current. The average current during electroosmosis experiments (averaged over a time period of 80 min) is plotted as a function of pH in Fig. 5C. These average currents are consistent with those observed in cyclic voltammetry experiments for microhole arrays at −1 V potential in Fig. 2B. Variation in current data is likely to be linked to some variation in the polymer film thickness deposited onto the array of microholes.

When expressing the water flux in terms of H_2O molecules per anion (the electroosmotic drag coefficient), a very clear trend emerges (Fig. 5D). The protonation of the PIM-EA-TB at a pH of 4 and lower clearly increases the current (see Fig. 5C) and therefore, given an approximately constant flux of water, the electroosmotic drag coefficient is reduced. Schematic illustrations of the effect are shown in Fig. 6. For pH > 4 only partial protonation of the PIM-EA-TB polymer occurs (Fig. 6A) and the mobile anions present in the micropores can move the trapped water. For pH < 4 a higher degree of protonation is achieved (Fig. 6B) and the conductivity of the anion-conducting PIM-EA-TB is increased (leading to higher currents). However, the amount of water transport remains similar as this could be associated with the total free volume available in the PIM-EA-TB microchannels. Therefore, the transport of water molecules per anion seems to be lower for higher currents. The chloride anions can be considered to behave like 'pistons' that push the water through the microporous material.

When the concentration of chloride in the PIM-EA-TB is low, the flow or electroosmotic drag coefficient appears to be higher. This situation is unusual (and linked to the molecular rigidity of the PIM-EA-TB) as the anions in this case cause substantial water flow and this can prevent the transport of cations in the opposite direction (see Fig. 6C). This result suggests that the apparent transference for anions and cations is linked to electroosmotic flow, i.e. the apparent transference for chloride is high as long as the flow is high. A further interesting point in this discussion is linked to the onset of the electroosmotic flow. There must be a point (e.g. making the pH more alkaline or employing other types of electrolytes) when a switch occurs from anion-dominated water transport to cation-dominated water transport. That is, the electroosmotic flow becomes bistable and is affected by small fluctuations at the beginning of the experiments.

4. Summary and conclusion

The observation of the high electroosmotic drag coefficient for low ion populations has been linked to a 'piston' mechanism associated with the anion movement in a molecularly rigid polymer of intrinsic microporosity, with the piston movement/direction controlled by the external potential. This observation raises questions connected to: (i) the dominating role of anion versus cation; (ii) the possibility of an 'inversion' in the water transport or bistability; (iii) the role of specific cations and anions, their concentrations, and their hydration radius/energy in the piston mechanism; (iv) the role of the microporous polymer design; (v) the role of small changes in hydrostatic pressure 'priming' the ion transport; and (vi) the role of other neutral species in solution. Some key conclusions are:

- The intrinsically microporous polymer PIM-EA-TB allows a high rate of water transport associated with the transport of ions (electroosmotic drag coefficients up to 4000 at neutral pH). This is likely to be linked to the molecularly rigid structure and could be of interest in electroosmotic pumps (e.g. for medical applications [32,33]), but also in water purification and water harvesting.
- The 'population' of mobile charge carriers in the microporous polymer offers a key to adjusting the electroosmotic drag coefficient, with lower populations causing an increase in the number of water molecules transported per charge carrier.
- Experimental observations for electroosmotic water transport in PIM-EA-TB are closely related to those for electroosmotic caffeic acid transport in PIM-EA-TB [34] where pH was shown to change the current without affecting the net rate of transport.
- Electroosmotic transport is usually linearly related to current [35]. Here, electroosmotic transport seems independent of changes in current when compared for different pH values, but this is linked to structural changes such as protonation modifying the membrane properties.

CRediT authorship contribution statement

Zhongkai Li: Data curation, Formal analysis, Investigation, Methodology. **Richard Malpass-Evans:** Data curation, Formal analysis, Investigation, Methodology, Writing - review & editing. **Neil B. McKeown:** Conceptualization, Funding acquisition, Methodology, Project administration, Resources, Supervision, Writing - review & editing. **Mariolino Carta:** Conceptualization, Funding acquisition, Investigation, Project administration, Resources, Supervision, Writing - review & editing. **Klaus Mathwig:** Conceptualization, Formal analysis, Investigation, Methodology, Resources, Software, Supervision, Writing - review & editing. **John P. Lowe:** Data curation, Formal analysis, Investigation, Methodology, Supervision, Writing - review & editing. **Frank Marken:** Conceptualization, Data curation, Funding acquisition, Investigation, Methodology, Supervision, Visualization, Writing - original draft.

Declaration of Competing Interest

The authors declare that they have no known competing financial interests or personal relationships that could have appeared to influence the work reported in this paper.

Acknowledgement

K.M. acknowledges financial support from Provincie Gelderland. F. M. is grateful for initial financial support by the EPSRC (EP/K004956/1).

References

[1] L.S. Zhong, L.M. Zhu, J.H. Li, W.L. Pei, H. Chen, S.M. Wang, A. Razaa, A. Khan, Y. P. Hou, Y.M. Zheng, Mol. Systems Design Engineer. (2021), https://doi.org/10.1039/d1me00019e.
[2] G.M. Geise, H.S. Lee, D.J. Miller, B.D. Freeman, J.E. Mcgrath, D.R. Paul, J. Polymer Sci. B 48 (2010) 1685–1718.
[3] A.A. Salehi, M. Ghannadi-Maragheh, M. Torab-Mostaedi, R. Torkaman, M. Asadollahzadeh, Renew. Sustain. Energy Rev. 120 (2020), 109627.
[4] E.T. Sayed, M. Al Radi, A. Ahmad, M.A. Abdelkareem, H. Alawadhi, M.A. Atieh, A. G. Olabi, Chemosphere 275 (2021), 130001.
[5] N. Mir, Y. Bicer, J. Environm, Management 289 (2021), 112496.
[6] I. Ihsanullah, M.A. Atieh, M. Sajid, M.K. Nazal, Sci. Total Environment 780 (2021), 146585.
[7] T.M. Zewdie, N.G. Habtu, A. Dutta, B. van der Bruggen, Water Reuse 11 (2021) 1–32.
[8] X.Y. Wang, C. Cheng, S.L. Wang, S.R. Liu, Microfluidics Nanofluidics 6 (2009) 145–162.
[9] A. Zlotorowicz R.V. Strand O.S. Burheim O. Wilhelmsen S. Kjelstrup J. Membrane Sci. 523 2017 402 408.
[10] T. Mabuchi T. Tokumasu Mechanical Engineer. J. 4 2017 UNSP 17–00054.
[11] R.K. Nagarale, A. Heller, W. Shin, J. Electrochem. Soc. 159 (2012) P14–P17.
[12] Z.X. Low, P.M. Budd, N.B. McKeown, D.A. Patterson, Chem. Rev. 118 (2018) 5871–5911.
[13] L.N. Wang, Y.Z. Zhao, B.B. Fan, M. Carta, R. Malpass-Evans, N.B. McKeown, F. Marken, Electrochem. Commun. 118 (2020), 106798.
[14] Y.Y. Rong, Q.L. Song, K. Mathwig, E. Madrid, D.P. He, R.G. Niemann, P. J. Cameron, S.E.C. Dale, S. Bending, M. Carta, R. Malpass-Evans, N.B. McKeown, F. Marken, Electrochem. Commun. 69 (2016) 41–45.

[15] E. Madrid, Y.Y. Rong, M. Carta, N.B. McKeown, R. Malpass-Evans, G.A. Attard, T. J. Clarke, S.H. Taylor, Y.T. Long, F. Marken, Angew. Chem. Inter. Ed. 53 (2014) 10751–10754.
[16] E. Madrid, P. Cottis, Y.Y. Rong, A.T. Rogers, J.M. Stone, R. Malpass-Evans, M. Carta, N.B. McKeown, F. Marken, J. Mater. Chem. A 3 (2015) 15849–15853.
[17] W.J. Lan, M.A. Edwards, L. Luo, R.T. Perera, X.J. Wu, C.R. Martin, H.S. White, Acc. Chem. Res. 49 (2016) 2605–2613.
[18] S.N. Bush, T.T. Volta, C.R. Martin, Nanomaterials 10 (2020) 571.
[19] J. Experton, X.J. Wu, C.R. Martin, Nanomaterials 7 (2017) 445.
[20] W. Shin, J.M. Lee, R.K. Nagarale, S.J. Shin, A. Heller, J. Am. Chem. Soc. 133 (2011) 2374–2377.
[21] Z. Peng, A. Morin, P. Huguet, P. Schott, J. Pauchet, J. Phys. Chem. B 115 (2011) 12835–12844.
[22] M. Carta, R. Malpass-Evans, M. Croad, Y. Rogan, J.C. Jansen, P. Bernardo, F. Bazzarelli, N.B. McKeown, Science 339 (2013) 303–307.
[23] B.R. Putra, M. Carta, R. Malpass-Evans, N.B. McKeown, F. Marken, Electrochim. Acta 258 (2017) 807–813.
[24] Y.Y. Rong, A. Kolodziej, E. Madrid, M. Carta, R. Malpass-Evans, N.B. McKeown, F. Marken, J. Electroanal. Chem. 779 (2016) 241–249.
[25] M. Ise, K.D. Kreuer, J. Maier, Solid State Ionics 125 (1999) 213–223.
[26] L. Tshwenya, F. Marken, K. Mathwig, O.A. Arotibe, A.C.S. Appl, Mater. Interface 12 (2020) 3214–3224.
[27] K.J. Aoki, L. Liu, F. Marken, J.Y. Chen, Electrochim. Acta 358 (2020), 136839.
[28] L. Liu, K.J. Aoki, J.Y. Chen, Electroanalysis (2021), https://doi.org/10.1002/elan.202100111.
[29] K. Amann-Winkel, M.C. Bellissent-Funel, L.E. Bove, T. Loerting, A. Nilsson, A. Paciaroni, D. Schlesinger, L. Skinner, Chem. Rev. 116 (2016) 7570–7589.
[30] M. Holz, S.R. Heil, A. Sacco, Phys. Chem. Chem. Phys. 2 (2000) 4740–4742.
[31] J.S. Murday, R.M. Cotts, J. Chem. Phys. 53 (1970) 4724–4725.
[32] N.M. Chola, S. Sreenath, B. Dave, R.K. Nagarale, Electrophoresis 40 (2019) 2979–2987.
[33] R.K. Nagarale, A. Heller, ChemElectroChem 1 (2014) 868–870.
[34] Z.K. Li, L.N. Wang, R. Malpass-Evans, M. Carta, N.B. McKeown, K. Mathwig, P. J. Fletcher, F. Marken, ChemElectroChem (2021), https://doi.org/10.1002/celc.202100432.
[35] K. Kontturi, L. Murtomaki, J.A. Manzanares, Ionic Transport Processes, Oxford University Press, Oxford, 2015, p. 212.